# Quantitative guiding of developmental cell fate transitions using gene-free modelling

Ismail Hajji[1], Eric D. Siggia[2], Francis Corson[3] & Wolfgang Keil*[1]

[1] Laboratoire de Physique des Cellules et Cancers, Institut Curie, PSL Research University, CNRS UMR168, Paris, France. Institut Pierre-Gilles de Gennes, Paris, France

[2] Center for Studies in Physics and Biology, The Rockefeller University, New York City, USA

[3] Laboratoire de Physique de l'Ecole Normale Supérieure, CNRS, ENS, Université PSL, Sorbonne Université, Université Paris Cité, Paris, France

*To whom correspondence should be addressed : wolfgang.keil@curie.fr

# Abstract

During development, cells gradually assume specialized fates via changes of transcriptional dynamics in thousands of genes. Terminal cell identities are then stabilized through the convergence of gene regulatory network dynamics and the accumulation of epigenetic DNA modifications. “Gene-free” (or geometric) modeling approaches for cell fate acquisition, which abstract from the underlying gene regulatory landscape and reason in phenotypic space, have been remarkably successful in explaining terminal fate outcomes. However, their implications for cellular dynamics during fate acquisition processes have so far not been tested *in vivo*. To do so, here we combine gene-free mathematical modeling of cell fate acquisition during *C. elegans* vulval development with temporally controlled perturbations of *in vivo* signaling dynamics using temperature sensitive (ts) mutant alleles of the EGF/Ras/MAPK and Notch signaling pathways. We show that gene-free modeling can quantitatively predict non-intuitive fate outcomes in a variety of ts genetic backgrounds, including pathway epistasis effects. In addition, we use gene-free modeling to infer how cell fate transitions can be guided towards specific outcomes through timed pulses of signaling activity and verify these model predictions quantitatively with temporally controlled signaling perturbations via temperature shifts in ts backgrounds. Our results highlight the predictive power of gene-free models beyond terminal fate outcomes and illustrate a new approach to quantitatively guide cell fate acquisition in a developmental context.

# Introduction

During development, cells proceed through a series of decisions between alternative cellular states to ultimately reach their final fates within the organism. Understanding, predicting, and manipulating cell fate has been a long-sought goal of developmental and regenerative biology. However, the determinants of cellular identities are exceedingly complex. The specification of different cell types from initially equivalent progenitors relies on the response to time-dependent signals, interpreted in a context-dependent manner through signaling cascades and gene regulatory networks that often involve dozens of molecular players. Recent technological advances are making it possible [1–5] to capture at single-cell resolution the genome-wide changes in transcriptional programs and epigenetic states that accompany cell state transitions, but deriving from such data an intuitive and predictive understanding of cell fate specification remains an open challenge.

C. H. Waddington contrasted the overwhelming complexity of molecular mechanisms with his nowadays omnipresent metaphor of the epigenetic landscape, in which developmental trajectories are likened to the motion of a ball rolling down a hill, with different valleys representing different fates. The landscape itself was envisaged as controlled by an underlying, web-like network of genes. In its essence, this metaphor captured the emergence of simplicity (a limited number of developmental outcomes) from a complex set of interacting molecular mechanisms. Giving a concrete mathematical form to this idea, several recent studies have shown that 'geometric' or 'gene-free' models - simple dynamical models that abstract away much of the underlying molecular complexity - allow both a general categorization of possible cellular decision structures, and an intuitive description and quantitative predictions for fate patterning in concrete systems [6–10]. In this approach, the general structure of the landscape, and a minimal parametrization, is postulated according to the known biology of a given system (e.g., so many valleys for so many possible fates), and the requisite quantitative parameters are then fit to experimental data. Although it ignores much of the underlying molecular details, this approach has been successfully applied to diverse systems, from pattern formation in a small group of cells in *Caenorhabditis elegans* (*C. elegans*) vulva [6,7], to self-organized patterning in *Drosophila* [8], metazoan segmentation [11], and the differentiation of mouse embryonic stem cells (mESCs) *in vitro* [12].

As a rather minimal instance that nonetheless embodies many general aspects of multicellular patterning, *C. elegans* vulval patterning provides an ideal context to pursue the implications of geometric models. The vulva is formed from a row of six vulval precursor cells (VPCs, called P3.p-P8.p) in the second and third larval stages (Fig. 1A). Each of the six VPCs has the potential to adopt any one of three different cell fates (called 1°, 2°, and 3°). In wild type (WT), an inductive signal originating from the anchor cell (AC) of the somatic gonad induces three cells (P5-7.p) in an invariant 2°1°2° pattern. These cells undergo three rounds of divisions to generate the vulval tissues, while the remaining three cells adopt the uninduced 3° fate, and fuse with the epidermal syncytium after one division (the complete fate pattern can thus be encoded as 3°-3°-2°-1°-2°-3°, or 332123 in short). P3.p quits the competence group in half of WT individuals. Vulval cell fates are specified via two conserved signaling pathways [13–18]: (i) the Ras/MAPK signaling pathway, activated by a Epidermal Growth Factor (EGF)-like ligand called LIN-3, secreted by the AC and (ii) lateral Delta-Notch signaling between neighboring VPCs via transmembrane (APX-1 and LAG-2) and diffusible (DSL-1) Notch ligands [19,20]. Briefly, EGF induces the 1˚ fate, which promotes expression of Notch ligands primarily in P6.p, inducing the 2˚ fate and repressing the 1˚ fate in the neighboring cells, P5.p and P7.p.

A simple gene-free model for vulval patterning, in which each cell travels in a two-dimensional landscape with three valleys (fates) was introduced in [6,7]. The landscape is independently tilted by EGF and Notch as development proceeds (Fig. 1C, see Materials & Methods for details). The initially equivalent VPCs start from the same location at the beginning of competence, but different signaling histories take them along different trajectories. The model also incorporates a stochastic term to allow for the inherent variability of cellular dynamics. The states of the VPCs in multiple repeats of a simulation can be represented as clouds of points traveling in the plane (Fig. 1E). Whereas in wild type, each of these clouds lies well within a valley at the end of competence, corresponding to an invariant fate pattern (Fig. 1D), perturbations affecting signaling can cause one or several clouds to lie across a boundary between valleys, accounting for partially penetrant phenotypes (variable fate patterns). This model reproduces a wide variety of VPC fate patterns of animals defective in the two signaling pathways. Notably, phenotypic epistasis arising from geometric effects alone could explain several non-intuitive cell fate outcomes that had previously been attributed to context-dependent pathway action via downstream effector switching [21] or direct inhibitory interactions between the EGFR-MAPK and Notch pathways [19,22,23].

Since geometric models for developmental patterning explicitly model the *dynamics* of cellular fate trajectories (Fig. 1E), they also make quantitative predictions for the impact of dynamical

perturbations (e.g., of cellular signaling) during the cell fate acquisition process. While this is one of their most powerful features, such predictions remain to be tested *in vivo*. The *in vitro* experiments performed in [12], while giving close to optimal external control over the signaling dynamics, hardly capture the full complexity of *in vivo* development, since endogenous Wnt secretion and FGF signaling dynamics were inhibited through small molecules, making cellular dynamics essentially cell autonomous. Thus, up to now, dynamical predictions of geometric models for multicellular patterning have not been challenged with quantitative *in vivo* measurements and perturbations *during* the differentiation process.

Here, we accomplish such tests, using vulval specification in *C. elegans* as a model system. We first construct combinations of mutants of the EGF/Ras/MAPK and Notch pathways with several alleles being strongly temperature sensitive (ts). We show that the gene-free model developed in [6,7], based on signaling parameters fit for the individual mutants, quantitatively captures these new allelic combinations at various growth temperatures. In doing so, we uncover new epistasis effects in the data that the model quantitatively explains without explicit pathway interactions. We then employ the temperature sensitivity of the allelic combinations to manipulate cell signaling during vulval cell fate acquisition using timed episodes of high and low cultivation temperatures. This allows us to 'guide' developmental trajectories towards predicted fate patterns, such as the maximal rescue of a mutant allele via a secondary mutation. The excellent agreement between the experimentally observed cell fate statistics and our theory demonstrates a general strategy to predictively control multicellular fate patterning *in vivo*.

# Results

## Gene-free parametrizations of genetic perturbations to the EGF and Notch signaling pathways

Our goal is to quantitatively guide *in vivo* vulval cell fate phenotypes in predictive ways by combining temperature-sensitive genetic perturbations of EGF/MAPK and Notch signaling activity with gene-free modelling of the underlying cell fate acquisition dynamics. Throughout this paper, we use the gene-free mathematical description proposed in [6,7] to model *C. elegans* vulval fate acquisition. In that description, the current state of each cell is represented by a position vector $\vec{r}$ in a two-dimensional 'fate plane', whose time evolution is given by

$$\frac{d\vec{r}}{dt} = \vec{v}(\vec{r}, s_1\vec{m}_1 + s_2\vec{m}_2) + \vec{\eta}(t) \quad (1)$$

In this equation, the vector field $\vec{v}$ (detailed in Methods) describes the 'landscape' in which the cell is 'moving', and its dependence on the EGF/MAPK and Notch signaling activity levels, $s_1$ and $s_2$, which in WT we equate with the ligand levels received by the cell, $l_1$ and $l_2$. The scalars $s_{1,2}$ multiply vectors $\vec{m}_{1,2}$ that are fixed for all genetic backgrounds. In addition to this deterministic term, the stochastic term $\vec{\eta}(t)$ builds in the inherent variability of cell dynamics and accounts for partially penetrant phenotypes (variable outcomes) observed in many conditions. A strong assumption of the model is that the effect of arbitrary signal levels is captured by the linear combination $s_1\vec{m}_1 + s_2\vec{m}_2$, which can be thought of as the 'force' with which the two signals 'push' the cell, in directions controlled by the vectorial parameters $\vec{m}_1$ and $\vec{m}_2$ (see Figure 1C). Thus, combined perturbations affecting the EGF/MAPK and Notch pathways (as in double mutants) are described by just combining the corresponding changes in the model parameters that represent ligand levels and signal transduction efficiency (as depicted in Figure 1F). Absent any explicit pathway coupling in the model, epistatic effects solely arise from the interplay between signaling responses and the underlying, nonlinear landscape.

For the EGF/MAPK pathway, WT ligand levels from the AC are described by a time-independent exponential gradient, i.e., a vector of ligand levels $l_1 = \{\gamma^3, \gamma^2, \gamma, 1, \gamma, \gamma^2\}$ for the six cells, where the parameter $\gamma < 1$ controls the sharpness of the gradient (see Materials and Methods) [6,7]. The perturbations considered here include mutations that affect ligand production by the AC, mutations that results in ectopic ligand production, and mutations affecting signal Ras/MAPK transduction efficiency. For the most general perturbation, the signal levels received by the six cells are given by

$$s_1 = L \cdot l_1 = L\,(\lambda \cdot \{\gamma^3, \gamma^2, \gamma, 1, \gamma, \gamma^2\} + \delta L + \delta l \cdot \{-3, -2, -1, 0, 1, 2\}) \quad (2)$$

Here, the prefactor $L$ represents signal transduction efficiency in the ERK pathway (e.g. SOS-1 in Fig. 1F) that modulates the response of all cells to all sources of ligands ($L = 1$ for WT and $L < 1$ for mutants in which signal transduction is impaired). Mutations affecting ligand production by the AC are represented by multiplying the WT gradient by a factor $\lambda$, whereas mutations that result in ectopic ligand production are represented by an additive term; experiments considered in the following require that we allow for non-uniform ectopic ligand levels, which for simplicity are assumed to exhibit a linear gradient, with offset $\delta L$ and slope $\delta l$.

As regards lateral Notch signaling, on the other hand, the emission of Notch ligand by each cell is a function its current state, described by a scalar function $L_2(\vec{r})$. The Notch ligand level $l_2$ to which each VPC is exposed includes contributions from its neighbors and from autocrine signaling. The only perturbation considered here is a mutation in *lin-12*/Notch that results in constitutive (ligand-independent) activation of the receptor, described as an additive contribution to signaling activity. Thus, in the most general case the Notch signaling activity of a cell (e.g. P6.p) is

$$s_2(P6.p) = l_2(P6.p) + N = L_2(P5.p) + \alpha L_2(P6.p) + L_2(P7.p) + N \qquad (3)$$

where $\alpha$ is the relative strength of autocrine vs. paracrine signaling, and $N$ describes ligand-independent activity (which is the same for every cell, with $N = 0$ in WT and $N > 0$ in the mutant).

**Quantitative Characterization of Temperature-Dependent Phenotypes for Vulval Patterning**

The parameters of our model, including the parameters that control its WT dynamics, as well as parameters representing several signaling mutants, e.g., the EGF hypomorph *lin-3(e1417)* [24], were previously fit to published data, and the same parameter values are used here. Our fits for different mutants had allowed us to make quantitative predictions for static perturbations such as double mutants. In addition, data from a temperature-sensitive mutant in which EGF ligand is ectopically produced, *lin-15(n765)* [25–27], had motivated qualitative predictions for time-dependent perturbations of EGF signaling [7] (in WT, LIN-15 transcriptionally represses lin-3/EGF in the hypodermis, limiting *lin-3* expression to the AC [26]; in mutants, LIN-3 levels are elevated throughout the hypodermal tissue, leading to ectopic induction of vulval cell fates; the predictions were qualitative because they were based on assuming an all-or-nothing EGF 'pulse', rather on a precise estimate of signaling shifts that could be achieved with a ts mutant).

Here, in order to use the model as a guide to implement controlled dynamic perturbations of vulval patterning, we first more precisely quantify and fit the terms of the model describing the phenotype of temperature-sensitive signaling mutants. To manipulate EGF and Notch signaling, we used the *lin-15(n765)* allele, mentioned above, as well as the *lin-12(n302)* allele, a weak gain-of-function mutation of the Notch receptor that results in ligand-independent activity [28–30]. Whereas *lin-12(n302)* is partially penetrant at the two temperatures considered here, 15ºC and 25ºC, ectopic EGF levels in the *lin-15(n765)* mutant at 25ºC are high enough that all VPCs are induced. In terms of the model, this only implies a lower bound on EGF levels at 25ºC. To infer a precise value, we

178 proceeded indirectly, by analyzing a cross between *lin-15(n765)* and a mutant in which EGF
179 signaling activity is reduced, *sos-1(cs41)*. *cs41* is a hypomorphic allele of the Guanine Nucleotide
180 Exchange Factor SOS-1, which is required for RAS-mediated signaling [31]; *cs41* is temperature
181 sensitive and we also analyzed it alone at different temperatures to quantify its effect on signaling
182 activity.

183 To quantify the phenotypes of these three mutants and crosses among them, VPC fate patterns
184 at two different temperatures (15ºC and 25ºC) were scored vulval fate patterns based on, progeny
185 number, cell positions and morphology of vulval invaginations in the early/mid L4 stage (Fig. 1E).
186 To aid with cell identification and progeny counting, two reporter genes, one labeling the AC and
187 the other labeling VPCs and their progeny, were crossed into the mutant strains (Fig. 1A, B; we
188 verified that these reporter transgenes do not affect EGF or Notch activity by scoring VPC fate
189 patterns in a sensitized background with reduced EGF, with and without the reporter genes, see
190 Suppl. Fig. 1). Wherever cell fates could not be unambiguously identified, we scored, and the
191 model was fit to, induced (1°/2° fate) vs. non-induced (3° fate) cells.

192 Contrary to what has been previously reported [21], we found that the *lin-15(n765)* mutant (in
193 which EGF is ectopically produced) is partially penetrant at 15ºC (Fig. 2A). Absent any indication
194 to the contrary, we had previously assumed a spatially uniform level of ectopic EGF when
195 modeling that mutant [6,7], and expected comparable induction levels for P3.p, P4.p, and P8.p
196 (Fig. 2B, left-hand panel). However, our observations showed a substantially higher induction of
197 the anterior cells, P3.p (54%) and P4.p (66%), compared to the posterior cell, P8.p (20%). We
198 first considered the possibility that this asymmetry results from a defect in the relative positioning
199 of the VPCs and AC, which has previously been reported to depend on EGF from the AC [32].
200 Based on the model, a shift in AC position was sufficient to bias P4.p vs. P8.p induction, but P3.p
201 induction remained negligible (Suppl. Fig. 2). Instead, our observations suggested that ectopic
202 EGF levels in *lin-15(n765)* must be non-uniform. Assuming for simplicity a linear gradient of
203 ectopic EGF, parameterized by the offset $\delta l$ and slope $\delta L$ in Eq. (2), we found that this was
204 sufficient to recapitulate the experimentally observed phenotype, with $\delta L \approx 0.18$ and $\delta l = 0.019$
205 (Fig. 2B-E). Based on the cross between *lin-15(n765)* and *sos-1(cs41)*, which showed only a
206 slight reduction in induction compared to *lin-15(n765)* alone (Suppl. Fig. 3), EGF signal
207 transduction is only mildly reduced by the *cs41* mutation at 15ºC (fit as $L \approx 0.85$; this is consistent
208 with the WT phenotype of *sos-1(cs41)* alone, since based on the model, reductions in EGF
209 signaling up to ~50% are phenotypically silent [6,7]).

210 At 25ºC, induction is almost entirely lost in *sos-1(cs41)* alone, implying a strong reduction of
211 function (fit as a reduction in signaling activity by a factor $L \approx 0.18$) (Fig. 2F-H). Since at 25ºC, the
212 *lin-15(n765)* mutant is fully induced, we used the cross between *lin-15(n765)* and *sos-1(cs41)* to
213 infer EGF levels in *lin-15(n765)* itself (Fig. 2J-L). Based on the phenotype of the cross, which
214 shows a partial rescue of induction, we then obtain a level of ectopic EGF $\delta L \approx 0.35$ for *lin-*
215 *15(n765)*, corresponding to about twice our fit for the level of ectopic EGF at 15ºC ; on the other
216 hand, our fits for the slope $\delta l$ at 15 and 25ºC do not significantly differ and we use the same value
217 $\delta l = 0.02$ in the following. Consistent with the phenotype of *lin-15(n765)* alone at 25ºC, the ectopic
218 EGF levels inferred indirectly from the *lin-15(n765) x sos-1(cs41)* phenotype are predicted to be
219 just sufficient for near-complete induction in *lin-15(n765)* alone, as seen in experiments (see the
220 second dashed line in Fig. 2B, right-hand panel).

221 As regards the Notch mutant *lin-12(n302)*, this has previously been described as a weak gain-of-
222 function mutation. Due to the role of Notch in the anchor cell vs. vulval uterine (AC/VU) fate
223 decision, *lin-12(n302)* animals lack an AC and therefore the source of the LIN-3/EGF inductive
224 signal, making them vulvaless (*vul*) [13,29,30]. With no AC and constitutive Notch activation, our
225 gene-free model predicts roughly equal levels of induction of all VPCs [6]. In contrast, we found
226 that: (i) induction of the central VPCs (P5-7.p) was higher than that of P3.p and P4.p, (ii) induction
227 levels were temperature sensitive, and (iii) more posterior VPCs were preferentially induced (Fig.
228 3A,B). Indeed, the average induction of P5-7.p at 15˚C was 10%, compared to 32% at 25˚C, and
229 P8.p was only (partially) induced at 25ºC, whereas P3.p and P4.p were never induced at any
230 temperature.

231 We reasoned that the higher induction levels of the central VPCs could result from residual *lin-3*
232 expression in the fate-transformed AC, potentially due to incomplete fate transformation.
233 Consistent with this, we occasionally observed expression of GFP from the *qyIs362* transgene in
234 the somatic gonad of *lin-12(n302)* animals, albeit much weaker than in wild-type animals (Suppl.
235 Fig. 4). This indicates that the promoter of the AC-specific transcription factor LIN-29, which
236 maintains *lag-2* expression in presumptive ACs, was transiently active in presumptive AC cells
237 for an extended period before cells eventually acquired the VU fate. The anteroposterior gradient
238 in induction levels at 25˚C most likely stems from subtle differences in VPC competence present
239 due to low overall EGF activity in this background. VPC competence is established through the
240 combined action of Wnt signaling (via the CWN-1 and EGL-20 ligands) and LIN-3/EGF [33]. EGL-
241 20 forms a long-range anteroposterior gradient across the animal with the source cells in the

242 animal tail [34]. We suspect that, at low EGF levels (due to the absence of an AC), a subtle AP
243 gradient of competence exists that makes posterior cells more sensitive to induction by ligand-
244 independent Notch activity.

245 To keep model parameters to a minimum, we sought to account for the *lin-12(n302)* phenotype
246 by fitting just two parameters, the prefactor $\lambda$ for the residual EGF gradient from the AC, and the
247 level $N$ of ligand-independent Notch activity (in doing so, we ignore the observed A-P asymmetry
248 in experimental outcomes - weak induction of P8.p at 25ºC vs. no induction of P3,4.p, as well as
249 the possible time dependence of residual EGF levels from the fate-transformed AC). Based on a
250 fit to our data, both residual EGF and ectopic N activity increase between 15º and 25ºC. The
251 changes in the inferred parameter values are relatively small, but being close to the threshold for
252 VPC induction, they are sufficient to result in appreciable changes in induction level (Fig. 3C-H).

253 In summary, we have quantitatively characterized the fate patterns of three ts alleles, *lin-15(n765)*,
254 *lin-12(n302)*, and *sos-1(cs41)*, that differentially affect *C. elegans* vulval patterning at various
255 cultivation temperatures. Model fits for permissive temperatures (phenotypically silent or fully
256 penetrant) were achieved through crosses with sensitized backgrounds, employing one of the key
257 strengths of the gene-free landscape model, i.e., its ability to predict fate patterns of mutant
258 combinations by simple parameter combination of the individual mutants. The model assumes
259 isotropic time-invariant Gaussian noise in cell-state (see Materials and Methods) and from that
260 noise was able to fit partial penetrance data in all cases by adjusting only deterministic
261 parameters. Thus, the gene-free landscape itself shapes the distribution of outcomes without the
262 need for additional spatiotemporal structure in the cell state noise. This characterization forms the
263 basis for pathway epistasis experiments (crosses between ts alleles and other alleles) as well as
264 time-dependent perturbation experiments, in which we vary the temperature during vulval fate
265 specification to provide time-dependent signaling activities.

266 **Successful Model Predictions for Epistasis Experiments Provide Insights into Cell Fate**
267 **Acquisition Dynamics**

268 From the parameter values for three mutant alleles in the EGF and Notch pathways, at 15˚C and
269 25˚C, the model now makes direct predictions (free of any additional parameters) for vulval fate
270 patterns in combinations of these alleles with each other as well as other previously characterized
271 mutants in the two pathways [6,7]. As a first test of model predictions, before moving to time-

272 dependent perturbations, we considered different allele combinations under a constant
273 temperature.

274 Focusing first on mutations in the EGF pathway alone, we considered the effect of ectopic EGF
275 in a background with reduced EGF from the AC, realized experimentally by crossing the *lin-*
276 *15(n765)* allele into the *lin-3(e1417)* background. *lin-3(e1417)* alone shows about 50% induction
277 of P6.p and very little induction of P5/7.p, a phenotype that was previously fit to a reduction of
278 EGF from the AC by a factor $\lambda \approx 0.28$. To examine the effect of ectopic EGF in this background,
279 we computed the outcome under increasing levels of uniform ectopic EGF (Suppl. Fig. 5A).
280 Strikingly, the model predicted that there is a 'sweet spot' just below $\delta l = 0.2$ where ectopic EGF
281 is sufficient to near fully rescue a WT fate for P5-7.p while causing very little ectopic induction of
282 the more distal cells (P3/4/8.p). This level happens to coincide with our fit for the *lin-15(n765)*
283 allele at 15ºC, allowing a direct test of the prediction. With allowance for an A-P gradient of ectopic
284 EGF, as inferred in *lin-15(n765)*, the model predicts rescue of P5-7.p and partial ectopic induction
285 of P3/4.p (Fig. 4B,C), in remarkable agreement with experimental outcomes (Fig. 4D).

286 Further supporting the model, and the notion that the EGF level at 15ºC is marginal for P5-7.p
287 rescue, a mild additional reduction in EGF signaling (through the *sos-1(cs41)* allele, fit as $L \approx 0.85$
288 at that temperature) results in less complete rescue of P5-7.p, as predicted (Fig. 4E-H).

289 In terms of the model, the rescue of the 2º fate in P5/7.p by ectopic EGF is explained by additional
290 Notch signaling from P6.p, which itself is more strongly induced to the 1º fate. The ectopic EGF
291 signaling received by P5/7.p can also synergize with Notch to induce the 2º fate (see [21,6,7]
292 and below), but simulations with ectopic EGF restricted to P6.p suggest that the dominant
293 contribution to the induction of P5/7.p is indirect, from enhanced Notch signaling form P6.p (Suppl.
294 Fig. 6).

295 Turning then to conditions in which both EGF and Notch signaling are perturbed, we considered
296 the effect of ectopic EGF in a background with ectopic (ligand-independent and uniform) Notch
297 activity, realized experimentally by a cross between *lin-12(n302)* and *lin-15(n765)*. A similar
298 condition was used previously to examine the synergy between EGF and Notch in the induction
299 of the 2º fate. Enhancement of 2º induction by low EGF signaling in a cross between another lin-
300 12 allele (*n379d*) and *lin-15(n765)* was interpreted to reveal a pro-2º effect of low EGF [21]. In
301 terms of our model, such a switch between pro-2º and pro-1º effect would require that the direction
302 in which EGF pushes cells vary with signal level, which we do not allow. Contrary to this

interpretation, our model shows that in the absence of any such change in direction, the interplay between EGF and the underlying cellular landscape (i.e., the cell-intrinsic dynamics) can give rise to a context-dependent response, with low EGF promoting a 2º or a 1º fate in different conditions.

In *lin-12(n302)* alone, P5-7.p are partially induced to a 2º fate, while the more distal cells are weakly or not induced (which we interpret as reflecting residual EGF signaling in animals lacking an AC; Fig. 3). When ectopic EGF is added (here also, we first consider uniform ectopic EGF), low levels of EGF (similar to *lin-15(n765)* at 15ºC) are predicted to result in the rescue of P5-7.p induction and a partial induction of more distal cells to the 2º fate (Suppl. Fig. 5B). In terms of the model, the enhanced induction of P5-7.p (which receive low residual EGF in the Notch mutant background) is similar to the rescue of the *lin-3(e1417)* mutant by ectopic EGF, while ectopic 2º fates in more distal VPCs manifest the above-mentioned synergy between low EGF and Notch in the induction of the 2º fate. If we allow for a gradient in ectopic EGF as fit for *lin-15(n765)*, at 15ºC P3/4.p are predicted to be more strongly induced and yield a mixture of 1º and 2º fates, whereas P8.p is more weakly induced (Fig. 4J-L). Although the experimental data do not show as marked an A-P asymmetry, they otherwise agree with model predictions, showing close to full induction of P5-7.p and partial induction in more distal cells (Fig. 4M; the difference between central and distal cells is as expected from the residual EGF in animals without an AC). At 25ºC, on the other hand, the ectopic EGF level from *lin-15(n765)* alone is sufficient to induce VPCs, and both model and experiments show near-complete induction in the cross (Fig. 4N-Q).

In summary, the two crosses considered here, with a marked difference in the induction of distal cells between 15º and 25ºC, thanks to the marked increase in ectopic EGF level (the variation in ectopic Notch activity in *lin-12(n302)* is smaller), lend themselves to dynamic perturbations through temperature shifts, and we can use the model, which correctly captures the outcomes at constant temperatures, to guide the choice of interesting perturbations.

**Guiding cell fates using dynamic perturbations of signaling**

So far, we have validated the model's predictions in terms of temporally static conditions in the genetic backgrounds and end-point phenotypes. As pointed out in (3), time-dependent perturbations of signaling activity during the competence period of precursors provide a much more sensitive test of how well geometric models can capture fate transition dynamics during development. In the model, these signaling time courses rapidly tilt the epigenetic landscape, diverting cells from their ongoing trajectories. Importantly, signaling dynamics, and thus fate

334 outcomes, can dramatically differ between conditions with identical integrated signaling activities,
335 depending on the timing of this diversion (Figs. 5 and 6). Viewed from the converse standpoint,
336 gene-free modeling can quantitatively predict how specific time courses of signaling may
337 dynamically guide cells towards increased or reduced induction levels or even specific fates.

338 The ts backgrounds characterized above provide an ideal means to test such dynamical
339 predictions *in vivo*. To do so, our approach was to shift populations of animals with ts mutations
340 at various timings and for various durations during competence from their permissive to their
341 restrictive temperatures (or vice versa). Since for each temperature, we have obtained parameter
342 fits, the model makes quantitative predictions for vulval fate patterns/induction levels as a function
343 of duration and timing of the temperature shifts without additional parameter fitting and making
344 very few assumptions (e.g., immediate parameter change and change of developmental speed
345 upon temperature shift, see Materials & Methods for details).

346 In the following, we focus on the induction of distal cells (P3/4/8.p), which as noted above (see
347 Fig. 4) shows the greatest variation between temperatures: in the two crosses, *lin-12(n302) x lin-*
348 *15(n765)* and *lin-3(e1417) x lin-15(n765)*, P5-7.p mostly adopt WT fates regardless of
349 temperature, whereas higher ectopic EGF yields higher induction of the more distal cells at 25ºC
350 compared to 15ºC.

351 In a cross with ectopic EGF in a background with reduced EGF from the AC, *lin-3(e1417) x lin-*
352 *15(n765*), the model predicts that an early pulse of high ectopic EGF (an early 25ºC pulse) is
353 much more effective than a late pulse at enhancing the induction of distal cells (Fig. 5A,B and
354 Suppl. Fig. 7A,B). This can largely be understood as the cell-autonomous effect of a signaling
355 pulse on a binary fate decision (the same effect would be recovered in a 1D model for the decision
356 of an isolated cell between two fates). Indeed, consider the cell under different levels of EGF.
357 Specifically, we first consider the fate trajectory of P8.p, which receives the lowest EGF levels
358 among VPCs and shows the sharpest response to pulses (Fig. 5B,C). Under low EGF
359 (corresponding to 15ºC) the initial state of P8.p in different simulation runs (except for rare outliers)
360 lies in the basin of attraction of the 3º fate, such that cells mostly adopt the 3º fate if EGF is held
361 constant. Under high EGF (corresponding to 25ºC), the 3º attractor has disappeared (undergoing
362 a saddle-node bifurcation with the 3º/1º saddle), such that all cells flow into the 1º attractor if EGF
363 is held constant. With a sufficiently long early pulse of high EGF, all cells will have moved past
364 the position of the 3º/1º separatrix that exists for low EGF (corresponding to 15ºC) and will thus
365 adopt the 1º fate even if EGF reverts to low level. By contrast, a late pulse will be much less

366 effective at converting cells that have moved previously towards the 3º attractor. The situation is
367 similar for P3,4.p, except that they receive a higher EGF level (and therefore show stronger
368 induction even at 15ºC), and, whereas Notch signaling between P3,4.p results in induction of 2º
369 as well as 1º fates (this is especially the case for P4.p, see Fig. 5B,C). In summary, the same
370 integrated dose of signal is predicted to displace fate outcomes much more effectively when
371 delivered early vs. late. This prediction is fully borne by experiments in which animals were shifted
372 from 15ºC to 25ºC and back at different times during competence (Fig. 5D and Suppl. Fig. 7A).
373 Importantly, to rule out the possibility that later pulses were less effective because they extended
374 beyond the period when VPCs are responsive, we ensured that the pulses lied within the
375 competence period, based on the timing of the first VPC divisions (see Materials & Methods).

376 In the case of ectopic EGF in a background with low ectopic Notch, *lin-12(n302) x lin-15(n765*),
377 the model similarly predicts that an early pulse is much more effective than a late pulse at
378 displacing the outcomes [7]. Specifically, an early pulse of high EGF can result in near-complete
379 induction of P3,4.p and P8.p, and the increase of induction compared to constant low EGF is
380 mostly in the form of 2º fates (compare Figs. 4K and 6B), at odds with the suggestion that EGF
381 can promote the 2º fate specifically at low levels [21]. It is noteworthy in this case (as contrasted
382 with the above case of ectopic EGF in an EGF hypomorph) that the predicted outcome of an early
383 pulse also markedly differs from that of a constant high EGF level, in which ectopic 1º fates
384 predominate (compare Figs. 4O and 6B). This further argues against the notion of an inherently
385 pro-1º or pro-2º signal. Consistent with our predictions, experiments in which animals were shifted
386 from 15ºC to 25ºC and back at different times during competence here also showed a much
387 stronger enhancement of induction by early vs. late pulses (Fig. 6D and Suppl. Fig. 7,D).

388 Together, our temperature shift/signaling pulse experiments provide a quantitative *in vivo* test of
389 a gene-free model with dynamic perturbations to cell signaling, both within a single signaling
390 pathway and involving pathway epistasis. They also show how a gene-free modeling approach
391 can provide intuitive explanations for cellular transition dynamics that inform strategies for how
392 fate transformation efficiencies can be improved with the right timing for pulsed signaling activities.

# 393 Discussion

394 Recent years have seen a surge of interest in giving the Waddington landscape a mathematical
395 foundation to test its predictive value with quantitative experimental data. By now, several studies

396 have shown that geometric or gene-free models, which abstract away much of the often system-
397 specific molecular details, provide a general framework to systematically classify possible
398 scenarios for cellular decisions [6,7,10,35], and are remarkably adept at capturing the essential
399 features of cellular decision making in concrete systems [8,12]. Apart from *in vitro* experiments in
400 'decoupled' mESCs (with no intercellular signaling) [12], experimental and theoretical studies
401 have so far focused on endpoint descriptions and static perturbations (mutant cell lines/strains).
402 Here, using classic ts alleles of the signaling pathways involved in *C. elegans* vulval patterning,
403 we developed an approach to directly demonstrate that geometric models can capture dynamic
404 cell-cell interactions, which are very relevant in the context of spatial patterning *in vivo*, but also
405 generically occur through ligand production and intrinsic signaling between initially equivalent
406 stem cells *in vitro*. We have shown that a previously developed gene-free model can capture
407 vulval fate patterns for several ts alleles of the EGF/Ras/MAPK and Notch pathway when raised
408 at either their permissive or restrictive temperatures. Model fits for phenotypically silent conditions
409 could be obtained by fitting crosses with sensitized genetic backgrounds, highlighting one of the
410 key predictive strengths of the model. When we then performed dynamic perturbation
411 experiments, by shifting populations of animals from permissive to restrictive and back to
412 permissive temperatures during precursor competence, the model correctly anticipated the
413 observed dependencies of fate patterns on the timing and duration of the temperature shift (i.e.,
414 of the signaling 'pulse'). Our results demonstrate a general approach that leverages interpretable
415 models to predictively guide individual cell fates and collective fate patterns, with obvious
416 implications for the rational engineering of tissues and organs, e.g., for regenerative medicine.

417 Beyond challenging model predictions against the eventual fate patterns, the predicted dynamics
418 could in many contexts be directly compared with data from adequate reporters. In the context of
419 vulval patterning, several reporters have been used previously to identify VPC fates, but they do
420 not systematically correlate with fate in partially penetrant backgrounds [36], making it unclear
421 that they provide a faithful readout of developmental trajectories. On the other hand, live sensors
422 for the ERK and N pathways have recently been developed, that could invite more dynamic
423 experiments, while keeping in mind the distinction between the pathway *activity* that we model
424 from the nuclear translocation of pathway effectors that is probed with these reporters. For the
425 EGF pathway, the activity of ERK, the most downstream protein kinase of the canonical Ras-Raf-
426 MEK-ERK cascade, has been monitored via a translocation reporter [37]. As in other model
427 systems [38–40], ERK activity was found to be pulsatile, with pulse frequency increasing with
428 increasing ligand levels. How this relates to upstream pathway *activity*, which our model purports

429 to describe, and is interpreted in the expression of the receiving genes, remains to be worked out.
430 For Notch activity, a biosensor called SALSA based on an endogenous tag of LIN-12 with a TEV
431 protease and co-expression of GFP-(TEV-cut-site)-RFP has recently been published [41]. One
432 key observation from this biosensor was the consistently higher sensor signal in P5/7.p vs. P6.p,
433 when our model predicts the highest Notch activity for P6.p. throughout competence (due to the
434 high ratio of autocrine to paracrine signaling, as required to account for the adoption of the 2º fate
435 by isolated cells upon ablation of all but one VPC [42–44]). Besides the ambiguities in terms of
436 the exact measure of pathway activity readout by the SALSA Notch sensor, we speculate that
437 elevated Notch activities in P5/7.p compared to P6.p may not be required for fate patterning but
438 rather features of fate execution. Indeed, a variation of our model that explicitly incorporated a
439 downregulation of Notch signaling in presumptive 1º cells allowed an eventual shutoff of autocrine
440 signaling, and a closer approach to the 1º fate attractor by those cells, but otherwise left the
441 dynamics of patterning and its response to perturbations largely unchanged [7].

442 Genetic screens over the past 40 years have likely uncovered a near-complete molecular parts
443 list underlying the specification and execution of VPC fates. With few exceptions, these
444 discoveries have been made by scoring endpoint fate phenotypes and clever genetic reasoning.
445 Live imaging and perturbations have seldom been used in this system, due to the technical
446 challenges of observing feeding, growing, and moving animals for extended periods at high
447 resolution. Recent advances in microfluidics for developing *C. elegans* larvae [45,46] should
448 render long-term observations and live manipulations during imaging feasible and promise to
449 open new avenues for quantitative studies of cell fate acquisition dynamics. We anticipate that,
450 through combinations of these imaging techniques with tools for real time manipulations of
451 signaling, e.g., via optogenetic control of protein localization [47–49], *C. elegans* vulval
452 development will continue to yield increasingly quantitative insights into *in vivo* cellular
453 differentiation.

454 **Table 1 - Model Fits**

| Allele | T(˚C) | VPC fates (% 1°, 2°, 3°) or (% induced, non-induced) | | | | | | Fitted Model Parameters | Reference for characterization |
|---|---|---|---|---|---|---|---|---|---|
| | | P3.p | P4.p | P5.p | P6.p | P7.p | P8.p | | |
| *lin-15*(*n765)* | 15˚C | 54,46 | 67,33 | 100,0 | 100,0 | 100,0 | 21,79 | $\delta L = 0.18$<br>$\delta I = -0.02$ | This study |
| | 25˚C | 100,0 | 100,0 | 100,0 | 100,0 | 100,0 | 100,0 | $\delta L = 0.35$<br>$\delta I = -0.02$ | This study |
| *sos-1(cs41)* | 15˚C | 0,0,100 | 0,0,100 | 0,100,0 | 0,0,100 | 0,100,0 | 0,0,100 | L = 0.85 | This study |
| | 25˚C | 0,0,100 | 0,0,100 | 0,0,100 | 4,0,96 | 0,0,100 | 0,0,100 | L = 0.18 | This study |
| *lin-3(e1417)* | | 0,0,100 | 0,0,100 | 0,10,90 | 54,0,46 | 0,10,90 | 0,0,100 | $\lambda = 0.28$ | (Corson & Siggia, 2017) |
| *lin-12(302)* | 15˚C | 54,46 | 67,33 | 100,0 | 100,0 | 100,0 | 21,79 | N = 0.13<br>$\lambda = 0.17$ | This study |
| | 25˚C | 100,0 | 100,0 | 100,0 | 100,0 | 100,0 | 100,0 | N = 0.145<br>$\lambda = 0.19$ | This study |

**Table 1: Summary of fate induction patterns and model parameter fits for EGF/Ras/MAPK and Notch alleles characterized in this study.** All alleles have *arTi85* I; *qyIs362* I in the background (see Materials & Methods for details).

# Materials and Methods

### *C. elegans* strains, general culture conditions & VPC fate scoring

A complete list of strains used in this study is given in Table 1. *C. elegans* stocks were maintained on 2.5% agar NGM (Nematode Growth Medium) plates (55mm diameter) seeded with *E. coli* strain OP50 at 20°C unless noted otherwise [50]. Mixed-age hermaphrodite stock cultures were hypochlorite-treated to obtain age-synchronized, arrested L1 larval populations [50]. All strains were raised at 15˚C and shifted to the indicated cultivation temperature upon feeding after L1 starvation arrest. To avoid the strong larval lethality of *sos-1(cs41)* at elevated temperatures, *sos-1(cs41)* animals were maintained at 15˚C for 30h after L1 starvation arrest (mid L2 stage) before being shifted to 25˚C. Following convention, we scored animals for VPC fates via Nomarski microscopy after cessation of vulval cell divisions (early/mid forth larval stage (L4). Previous studies used the number of progenies, axis of cell divisions, adherence to the ventral cuticle, overall morphology of the vulval tissue gathered from Nomarski microscopy as hallmarks of fate choice [17,18]. We found cell-fate assignment in *muv* strains based on those criteria highly ambiguous. Therefore, we crossed all characterized alleles into transgenes *arTi85* [lin-31p::ERK::KTR::mClover::T2A::mCherry::his-11::unc-54 3'UTR + rps-27p::NeoR::unc-54 3'UTR] and *qyIs362*[lin-29p::GFP]. *arTi85* includes a histone H2B mCherry tag, expressed in VPCs and its descendants (Fig. 1A). *qyIs362* is an AC-specific cytoplasmic GFP reporter, allowing unambiguous identification of the AC in confocal stacks (Fig. 1A). The strain NK1382, harboring *qyIs362* and *qyIs17 [zmp-1p::mCherry]* II [51], was outcrossed, to obtain our *qyIs362* background WT strain OS11953 (see Table 1).

### Model formulation and implementation

The geometric model [6,7], describes the state of each VPC by a vector $\vec{r}$ in two-dimensional space (Fig. 1C) and its dynamics by the stochastic differential equation

$$\frac{d\vec{r}}{dt} = \frac{1}{\tau}\left[\vec{\sigma}_1\left(\vec{f} + \vec{m}\right) - \vec{r}\right] + \vec{\eta}(t),$$

where $\vec{f}(\vec{r}) = 2\vec{r} - x\,y\,\vec{e}_x + (\mathrm{y}^2 - \mathrm{x}^2)\,\vec{e}_y$ is a polynomial vector field with threefold symmetry and the nonlinear function

$$\vec{\sigma}(\vec{r}) = \tanh\|\vec{f}\|\frac{\vec{f}}{\|\vec{f}\|}$$

ensures that the dynamics is bounded. The term $\vec{m} = \vec{m}_0 + l_1\vec{m}_1 + l_2\vec{m}_2$ integrates a bias towards the default 3° fate, $\vec{m}_0$, and the effect of EGF and Notch signaling, parameterized by two vectors, $\vec{m}_1$ and $\vec{m}_2$, which are combined linearly according to the levels of EGF and Notch ligands, $l_1$ and $l_2$ on the cell (see main text). Variability in the dynamics is described by the stochastic term $\vec{\eta}(t)$, parameterized by a coefficient of diffusion *D* in phase space,

$$\eta_i(t)\eta_j(t') = 2D\delta_{ij}(t - t') .$$

A fixed exponential gradient of EGF is assumed

$$l_1 = \{\gamma^3, \gamma^2, \gamma, 1, \gamma, \gamma^2\}$$

while the level of Notch ligands a cell exposes to its neighbors is a function of its current state

$$L_2(\vec{r}) = \sigma_2(n_0 + \vec{n}_1\vec{r})$$

and varies continuously from 0 to 1 across a line parameterized by $n_0$ and $n$ (Fig. 1C, bottom right). Stochastic simulations of the model were performed as described in [6].

**Parameter fitting**

All model parameter values were taken from [7], except noted otherwise. Ligand levels were fit to the proportions of the different fates, 1°−3°, adopted by each cell, P3-8.p, in different conditions (correlations between cells are thus ignored; as in [6], the fit minimizes the sum of squares of the difference between fate proportions in model and experiment). For conditions in which we were unable to distinguish between 1° and 2° fates (e.g., *lin-15(n765)*), we fit the fraction that each cell adopted either 1° or 2° fate in the model. As an exception to this general procedure, the model was fit to the *lin-12(n302)* allele at 15ºC based on the average fate proportions among two groups of cells, P4,8.p and P5-7.p (fit in this way, the model captures the higher induction of central VPCs but exhibits highest induction in P6.p, at odds with the experimental data, see Fig. 3A,C; when it was fit to the full fate pattern, it failed to capture any difference within the VPCs, yielding uniformly low induction).

**Inferring timing and duration of signaling perturbations via temperature shifts**

Inferring the timing and duration of signaling perturbations via temperature shifts requires an estimation for how much “Developmental time” has passed in each absolute time and, ultimately, what fraction of competence was spent at which temperature. In the following,

upper case times indicate "Developmental time" in **model time units**, lower case times indicate **absolute** times in hours. We define:

- $v_0$ ... developmental speed at 15˚C, measured in "(developmental time)/h".
- $\alpha$ … dimensionless scaling factor for developmental pace at 25˚C vs. 15˚C, so that $v_{25^\circ C} = \alpha v_0$. For WT *C. elegans* animals, $\alpha$ can be inferred comes from the Arrhenius law for developmental rate of *C. elegans* (37). For other genotypes, e.g., *lin-3(e1417)* x *lin-15(n765)*, we measured developmental progression at 25˚C vs. 15˚C through staging age-synchronized populations at various absolute times of development in the L3 and L4 stages. $\alpha$ was found to be ~1.4 for all strains.
- $a$ ... acceleration in developmental speed after temperature switch, measured in "(developmental speed)/h". We assume that acceleration is linear and $\alpha = \gamma v_0$ with $\gamma$ in units of 1/h. This formulation assumes that all worms take the same **absolute** time to increase their own developmental speed by a certain factor, i.e., faster developing worms accelerate at a faster absolute rate.

We define the absolute times $t_1, t_2, t_3, t_4$ as the time spent at 15˚C, time spent accelerating to 25˚C developmental rate, time spent at 25˚C, and time at 15˚C developmental rate (assuming instantaneous deceleration), the total developmental time passed when the animal is scored is given by

$$T_{total} = v_0 t_1 + v_0 t_2 + \frac{a}{2} t_2^2 + \alpha v_0 t_3 + v_0 t_4.$$

From the experiment, known are the absolute times $t_1$, $t_{pulse} = t_2 + t_3$ , and $t_4$. With the assumptions above, $t_2 = \alpha/\gamma$. Solving the equation for $T_{total}$ for $v_0$ gives the developmental time (model time) passed per hour at 15˚C. From this, one can calculate how much developmental time has passed in all temperature phases of the experiment.

In line with prior work, we assumed VPC competence to last from the mid L2 stage until shortlt after the first VPC division, which we determined to be at 1/3 in the L3 stage in WT, *sos-1(cs41)* and *lin-3(e1417)* (data not shown). This developmental time span corresponds to the model time interval [0,1]. In line with recent studies on temporal scaling in *C. elegans* post-embryonic development [52], we assumed that all animals have the same relative duration of each larval stage, independent of their individual developmental pace. Furthermore, we assumed that animals immediately shift developmental pace upon temperature shifts (i.e., $t_2 = 0$). To ensure that the late temperature pulses were delivered within the VPC competence window, we verified in a subset of the populations that, at the time points of the temperature

down shifts, VPCs had not undergone their first round of division in the vast majority of animals.

## Data availability

All strains used in this study (Table 1) are available upon request.


## Funding

W.K. was funded by the CNRS ATIP/Avenir program and the Conseil Regional d'Île de France (DIM ELICIT-AAP-2020, 20002719). F.C. and W.K received support by the Q-Life initiative at PSL Research University, Paris, FRANCE (Q-life ANR-17-CONV-0005). W.K. acknowledges additional support by the Centre National de la Recherche Scientifique (CNRS) and Institut Curie.

## Acknowledgments

We thank David Sherwood for sharing the NK1382 strain ahead of publication. We thank Rémy Fert and Giacomo Gropplero (Institut Curie) for help in building a custom temperature-control system on our microscope. We thank Shai Shaham, members of Shaham lab (The Rockefeller University) for feedback during the early stages of this project. We thank Marie-Anne Félix (ENS, Paris) for advice on VPC fate scoring. We are grateful to all members of the Keil lab for fruitful discussions and feedback throughout this project.


## Author contributions

EDS, FC, and WK conceived and designed the project. IH and WK performed all experiments, supervised by WK. IH, FC, and WK analyzed the data. All authors wrote and edited the manuscript.

## Competing interests

The authors declare that no competing interests exist.

# Bibliography


[1] J. Cao, J. S. Packer, V. Ramani, D. A. Cusanovich, C. Huynh, R. Daza, X. Qiu, C. Lee, S. N. Furlan, F. J. Steemers, A. Adey, R. H. Waterston, C. Trapnell, and J. Shendure, Science **357**, 661 (2017).

[2] J. Cao, M. Spielmann, X. Qiu, X. Huang, D. M. Ibrahim, A. J. Hill, F. Zhang, S. Mundlos, L. Christiansen, F. J. Steemers, C. Trapnell, and J. Shendure, Nature **566**, 496 (2019).

[3] L. M. Saunders, S. R. Srivatsan, M. Duran, M. W. Dorrity, B. Ewing, T. Linbo, J. Shendure, D. W. Raible, C. B. Moens, D. Kimelman, and C. Trapnell, Deep Molecular, Cellular and Temporal Phenotyping of Developmental Perturbations at Whole Organism Scale, preprint, Genomics, 2022.

[4] L. M. Saunders, S. R. Srivatsan, M. Duran, M. W. Dorrity, B. Ewing, T. H. Linbo, J. Shendure, D. W. Raible, C. B. Moens, D. Kimelman, and C. Trapnell, Nature **623**, 782 (2023).

[5] X. Huang, J. Henck, C. Qiu, V. K. A. Sreenivasan, S. Balachandran, O. V. Amarie, M. Hrabě De Angelis, R. Y. Behncke, W.-L. Chan, A. Despang, D. E. Dickel, M. Duran, A. Feuchtinger, H. Fuchs, V. Gailus-Durner, N. Haag, R. Hägerling, N. Hansmeier, F. Hennig, C. Marshall, S. Rajderkar, A. Ringel, M. Robson, L. M. Saunders, P. Da Silva-Buttkus, N. Spielmann, S. R. Srivatsan, S. Ulferts, L. Wittler, Y. Zhu, V. M. Kalscheuer, D. M. Ibrahim, I. Kurth, U. Kornak, A. Visel, L. A. Pennacchio, D. R. Beier, C. Trapnell, J. Cao, J. Shendure, and M. Spielmann, Nature **623**, 772 (2023).

[6] F. Corson and E. D. Siggia, Proceedings of the National Academy of Sciences of the United States of America **109**, 5568 (2012).

[7] F. Corson and E. D. Siggia, eLife **6**, (2017).

[8] F. Corson, L. Couturier, H. Rouault, K. Mazouni, and F. Schweisguth, Science **356**, (2017).

[9] A. Raju and E. D. Siggia, A Geometrical Model of Cell Fate Specification in the Mouse Blastocyst, preprint, Developmental Biology, 2023.

[10] M. Sáez, J. Briscoe, and D. A. Rand, Interface Focus. **12**, 20220002 (2022).

[11] L. Jutras-Dubé, E. El-Sherif, and P. François, eLife **9**, e55778 (2020).

[12] M. Sáez, R. Blassberg, E. Camacho-Aguilar, E. D. Siggia, D. A. Rand, and J. Briscoe, Cell Systems **13**, 12 (2022).

[13] I. S. Greenwald, P. W. Sternberg, and H. R. Horvitz, Cell **34**, 435 (1983).

[14] P. W. Sternberg and H. R. Horvitz, Cell **44**, 761 (1986).

[15] P. W. Sternberg, Nature **335**, 551 (1988).

[16] E. L. Ferguson, P. W. Sternberg, and H. R. Horvitz, Nature **326**, 259 (1987).

[17] P. W. Sternberg and H. R. Horvitz, Cell **58**, 679 (1989).

[18] R. J. Hill and P. W. Sternberg, Nature **6386**, 470 (1992).

[19] D. D. Shaye and I. Greenwald, Nature **420**, 686 (2002).

[20] N. Chen and I. Greenwald, Developmental Cell **6**, 183 (2004).

[21] T. P. Zand, D. J. Reiner, and C. J. Der, Developmental Cell **20**, 84 (2011).

[22] A. S. Yoo and I. Greenwald, Science **310**, 1330 (2005).

[23] T. Berset, E. F. Hoier, G. Battu, S. Canevascini, and A. Hajnal, Science **291**, 1055 (2001).

[24] B. J. Hwang and P. W. Sternberg, Development **131**, 143 (2004).

[25] S. G. Clark, X. Lu, and H. R. Horvitz, Genetics **137**, 987 (1994).

[26] M. Cui, J. Chen, T. R. Myers, B. J. Hwang, P. W. Sternberg, I. Greenwald, and M. Han, Developmental Cell **10**, 667 (2006).

[27] M. Cui, M. A. Allen, A. Larsen, M. MacMorris, M. Han, and T. Blumenthal, Proc. Natl. Acad. Sci. U.S.A. **105**, 16665 (2008).

[28] M. Sundaram and I. Greenwald, Genetics **135**, 755 (1993).

[29] M. Sundaram and I. Greenwald, Genetics **135**, 765 (1993).

[30] R. S. Underwood, Y. Deng, and I. Greenwald, Genetics **207**, 1473 (2017).

[31] C. Chang, The EMBO Journal **19**, 3283 (2000).

[32] S. Grimbert, K. Tietze, M. Barkoulas, P. W. Sternberg, M.-A. Félix, and C. Braendle, Developmental Biology **416**, 123 (2016).

[33] T. R. Myers and I. Greenwald, Proceedings of the National Academy of Sciences of the United States of America **104**, 20368 (2007).

[34] A. M. Pani and B. Goldstein, eLife **7**, e38325 (2018).

[35] D. A. Rand, A. Raju, M. Sáez, F. Corson, and E. D. Siggia, Proc. Natl. Acad. Sci. U.S.A. **118**, e2109729118 (2021).

[36] M. Cui and M. Han, Developmental Biology **257**, 104 (2003).

[37] C. de la Cova, R. Townley, S. Regot, and I. Greenwald, Developmental Cell **42**, 542 (2017).

[38] K. Aoki, Y. Kumagai, A. Sakurai, N. Komatsu, Y. Fujita, C. Shionyu, and M. Matsuda, Molecular Cell **52**, 529 (2013).

[39] J. G. Albeck, G. B. Mills, and J. S. Brugge, Molecular Cell **49**, 249 (2013).

[40] B. Sparta, M. Pargett, M. Minguet, K. Distor, G. Bell, and J. G. Albeck, Journal of Biological Chemistry **290**, 24784 (2015).

[41] J. M. Shaffer and I. Greenwald, Developmental Cell **57**, 930 (2022).

[42] E. Hoyos, K. Kim, J. Milloz, M. Barkoulas, J.-B. Pénigault, E. Munro, and M.-A. Félix, Curr Biol **21**, 527 (2011).

[43] W. S. Katz, R. J. Hill, T. R. Clandinin, and P. W. Sternberg, Cell **82**, 297 (1995).

[44] J. Kimble, (1981).

[45] W. Keil, L. M. Kutscher, S. Shaham, and E. D. Siggia, Developmental Cell **40**, 1 (2017).

[46] S. Berger, S. Spiri, A. deMello, and A. Hajnal, Development **148**, dev199674 (2021).

[47] F. Di Pietro, S. Herszterg, A. Huang, F. Bosveld, C. Alexandre, L. Sancéré, S. Pelletier, A. Joudat, V. Kapoor, J.-P. Vincent, and Y. Bellaïche, Developmental Cell **56**, 3393 (2021).

[48] A. M. Dowbaj, R. P. Jenkins, D. Williamson, J. M. Heddleston, A. Ciccarelli, T. Fallesen, K. M. Hahn, R. D. O'Dea, J. R. King, M. Montagner, and E. Sahai, Journal of Cell Science **134**, jcs253484 (2021).

[49] A. P. Singh, P. Wu, S. Ryabichko, J. Raimundo, M. Swan, E. Wieschaus, T. Gregor, and J. E. Toettcher, Cell Reports **38**, 110543 (2022).

[50] T. Stiernagle, *Maintance of C. Elegans* (1999), pp. 51–67.

[51] D. S. Costa, I. W. Kenny-Ganzert, Q. Chi, K. Park, L. C. Kelley, A. Garde, D. Q. Matus, J. Park, S. Yogev, B. Goldstein, T. V. Gibney, A. M. Pani, and D. R. Sherwood, Development **150**, dev201570 (2023).

[52] O. Filina, B. Demirbas, R. Haagmans, and J. S. Van Zon, Proc. Natl. Acad. Sci. U.S.A. **119**, e2123110119 (2022).

[53] M. Barkoulas, J. S. van Zon, J. Milloz, A. van Oudenaarden, and M.-A. Félix, Developmental Cell **24**, 64 (2013).

[54] C. Braendle and M.-A. Félix, Developmental Cell **15**, 714 (2008).

# Figures

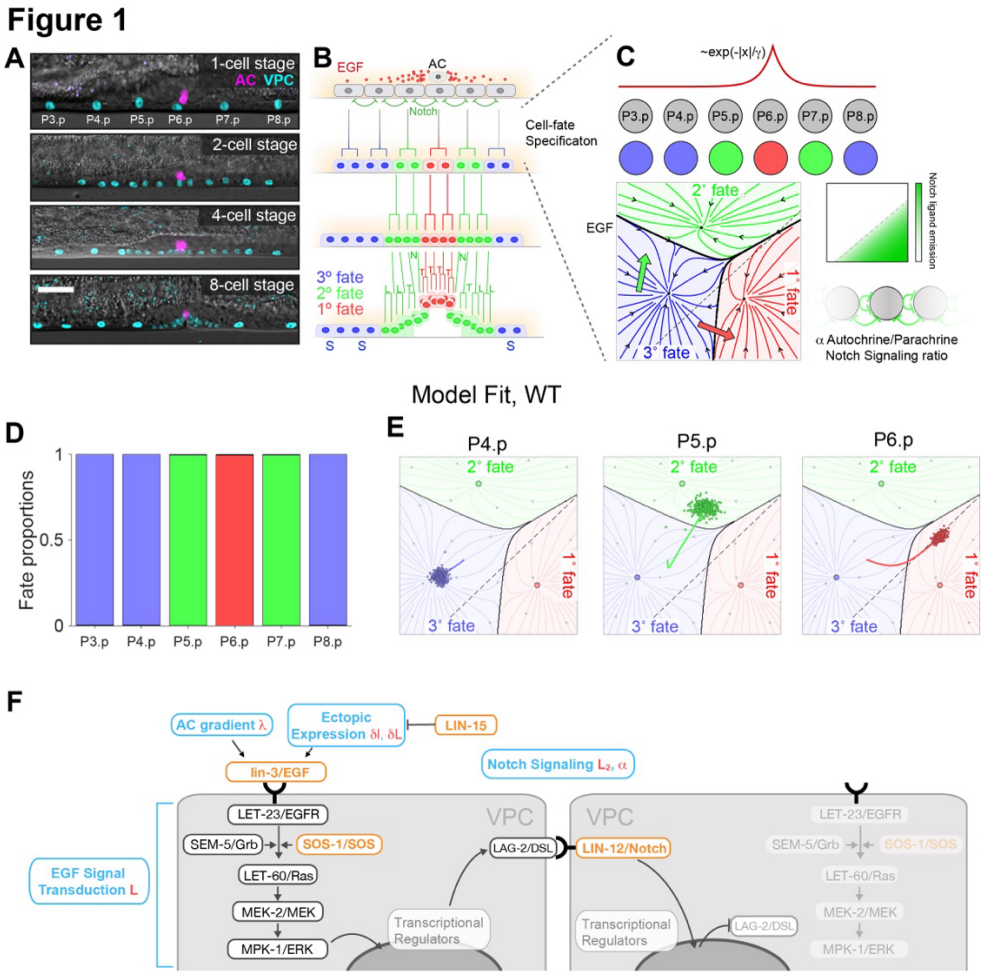


**Figure 1: Cell-fate acquisition during *C. elegans* vulval development.** (**A**, **B**) Micrographs (**A**) and schematics (**B**) of *C. elegans* of vulval development. (**A**) The transgene *arTi85* [*lin-31p*::*ERK-KTR*(*NLS3*)-*mClover-T2A-mCherry-H2B*::*unc-54 3'UTR*] (1) (cyan) labels vulval precursor cells and descendants throughout all stages of vulval development, *qyIs362 [lin-29A/B>GFP]* (magenta) brightly labels the anchor cell starting from the mid L2 larval stage. Together, they allow accurate location of VPCs and scoring of vulval fate induction. (**B**) The vulva forms from a row of six precursor cells (VPCs), P3.p–P8.p, which are competent to adopt three possible fates, inner vulval or primary (1°), outer vulval or secondary (2°), and non-vulval or tertiary (3°). Fates are identified by characteristic cell division patterns (the orientation of terminal divisions is indicated by letters: L, longitudinal; T, transverse; N, undivided; S, fused with the epidermal syncytium; underlined cells are adhered to the cuticle). In WT, a graded EGF signal from the anchor cell and lateral Notch signaling among VPCs (green arrows) specify an invariant pattern of fates, 32123. (**C**) Top, Our gene-free model assumes an exponential EGF gradient originating from the AC, and autocrine and paracrine Notch signaling produced by the VPCs according to their current state. Bottom, Two-dimensional fate plane of the gene-free model for vulval fate specification [6,7] . Black dots indicate valleys of the landscape, and black arrowheads the direction of cell state flow. Colored lines indicate cell fate basins (red, 1º fate; green, 2º fate; blue, 3º fate), separated by black lines. The dashed line is where Notch ligand expression is half maximum (see also green color code in inset, right). (**D**) Fate proportions for the six VPCs in the model. (**E**) Model fate trajectories for WT VPCs (200 realizations; lines and dots show average trajectories and individual outcomes, colored according to the WT fate of each cell as per **C**). (**F**) Diagram of EGF and Notch signaling pathways, showing how different genetic perturbations characterized in this paper translate to changes in model parameters.

# Figure 2

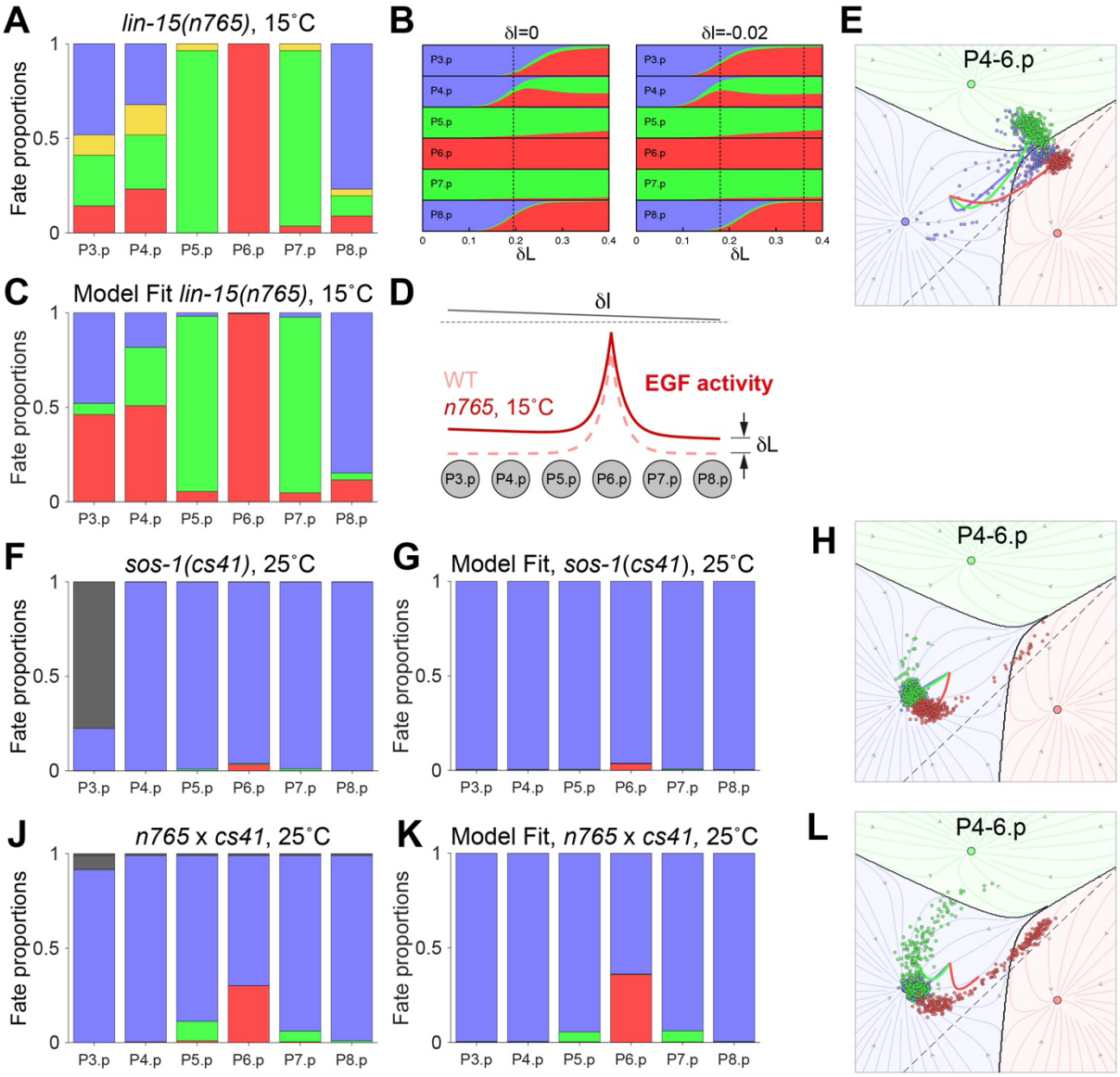


**Figure 2: Quantitative analysis and parametrization of temperature-sensitive mutant alleles affecting EGF signaling.** (**A**) Fate proportions in the *lin-15*(*n765*) mutant at 15ºC (N=39 animals). (**B**) Fate proportions in the model as a function of ectopic EGF level $\delta L$, with (right, $\delta l = -0.02$) or without (left, $\delta l = 0$) an A-P gradient in ectopic EGF levels. Dashed lines show model fits to data from **A** (and for the same allele at 25ºC in right-hand panel). (**C-E**) Illustration of model fit to the *lin-15*(*n765*) mutant at 15ºC, showing the fate proportions (**C**), EGF gradient (**D**), and fate trajectories of P4-6.p (**E**; average trajectories and individual outcomes colored according to the WT fate of each cell, cf. Fig. 1E). (**F-H**) Experimental fate proportions (**F**; black filling indicates animals in which P3.p did not become competent), and model fate proportions (**G**) and trajectories (**H**) for the *sos-1*(*cs41*) mutant at 25ºC. (**J-L**) Same as (**F-H**) for the *lin-15*(*n765*) *x sos-1*(*cs41*) cross at 25ºC.

## Figure 3

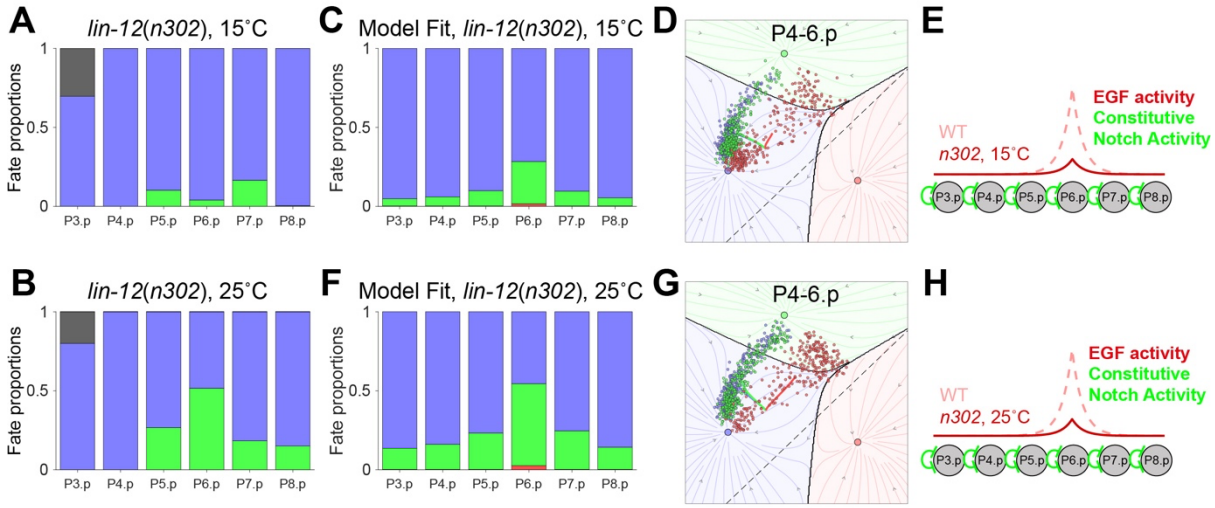


**Figure 3: Quantitative analysis and parametrization of a temperature-sensitive Notch mutant allele.** (**A**) Fate proportions in the *lin-12*(*n302)* mutant at 15ºC (N=112). (**C-E**) Illustration of model fit to the *lin-12*(*n302)* mutant at 15ºC, showing the fate proportions (**C**), fate trajectories (**D**), and signaling activity (including residual EGF and constitutive Notch activity). (**B**,**F-H**) Same as (**A,C-E**) for the *lin-12*(*n302)* mutant at 25ºC.

## Figure 4

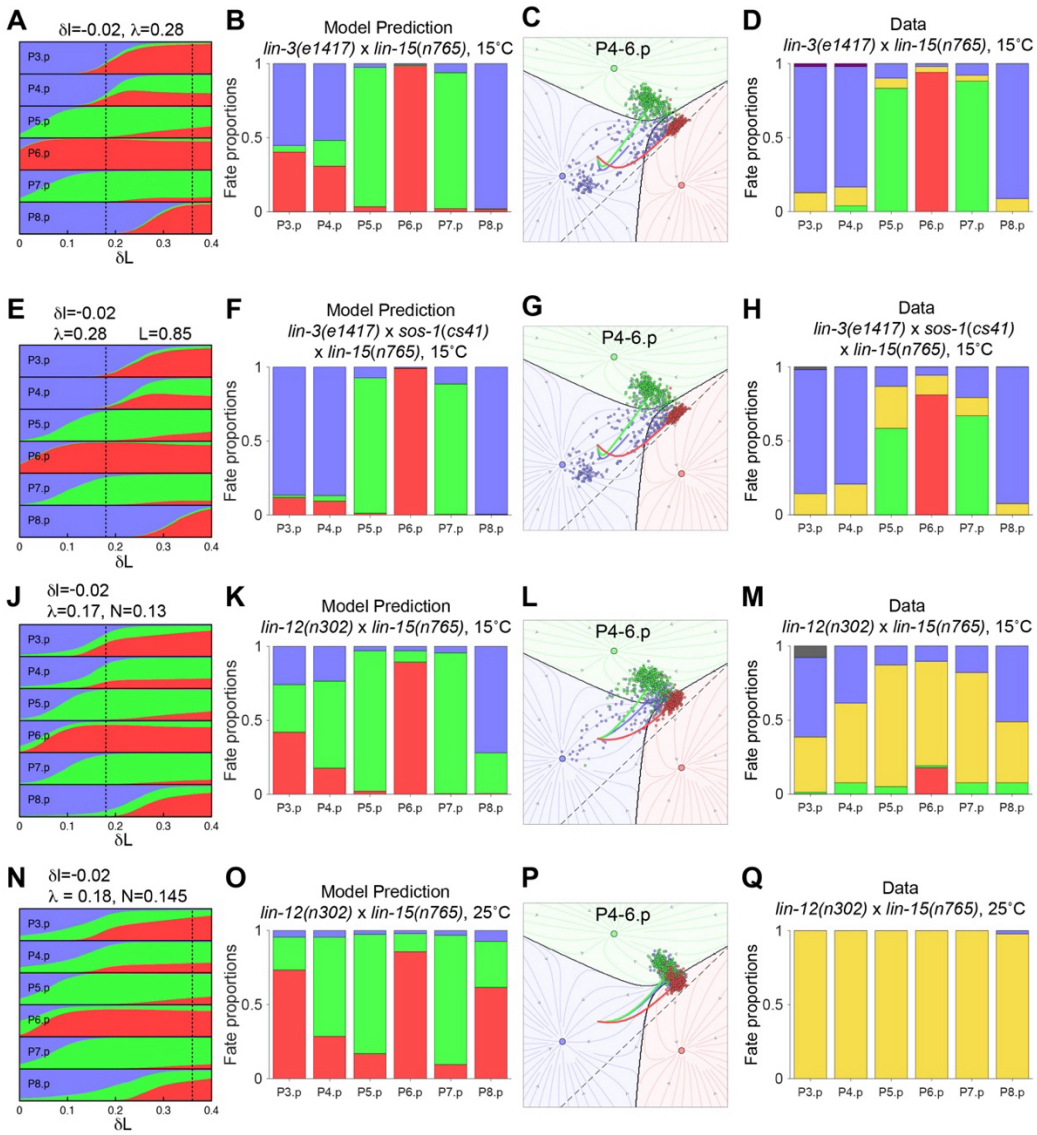


**Figure 4: The geometric model quantitatively predicts epistasis of temperature-sensitive alleles.** Model predictions are compared with experimental outcomes for crosses between the *lin-15*(*n765*) allele and other mutants within the EGF pathway (**A-H**) and in the Notch pathway (**J-Q**). In each row, corresponding to a given background and temperature, the first column shows the predicted fate proportions in the model as a function of ectopic EGF level $\delta L$ in that background, with a fixed slope $\delta l = -0.02$ (**A-D**, *lin-3*(*e1417*); **E**, *sos-1*(*cs41*) *x lin-3*(*e1417*); **J**, **N**, *lin-12*(*n302*)). The following columns show the predicted fate proportions (**B**, **F**, **K**, **O**), predicted fate trajectories (**C**, **G**, **L**, **P**), and experimental fate proportions (**D**, **H**, **M**, **Q**) for the crosses at the indicated temperatures. The dashed lines in (**A**, **E**, **J**, **N**) show our fits for *lin-15*(*n765*) at the relevant temperature, 15ºC or 25ºC (*lin-3*(*e1417*) is not temperature-sensitive and the 25ºC line is also included in **A** to show the prediction for the cross at that temperature). In experiments, the 1º and 2º fates could not always be distinguished, and some cells were only scored as induced (yellow) or non-induced (blue).

# Figure 5

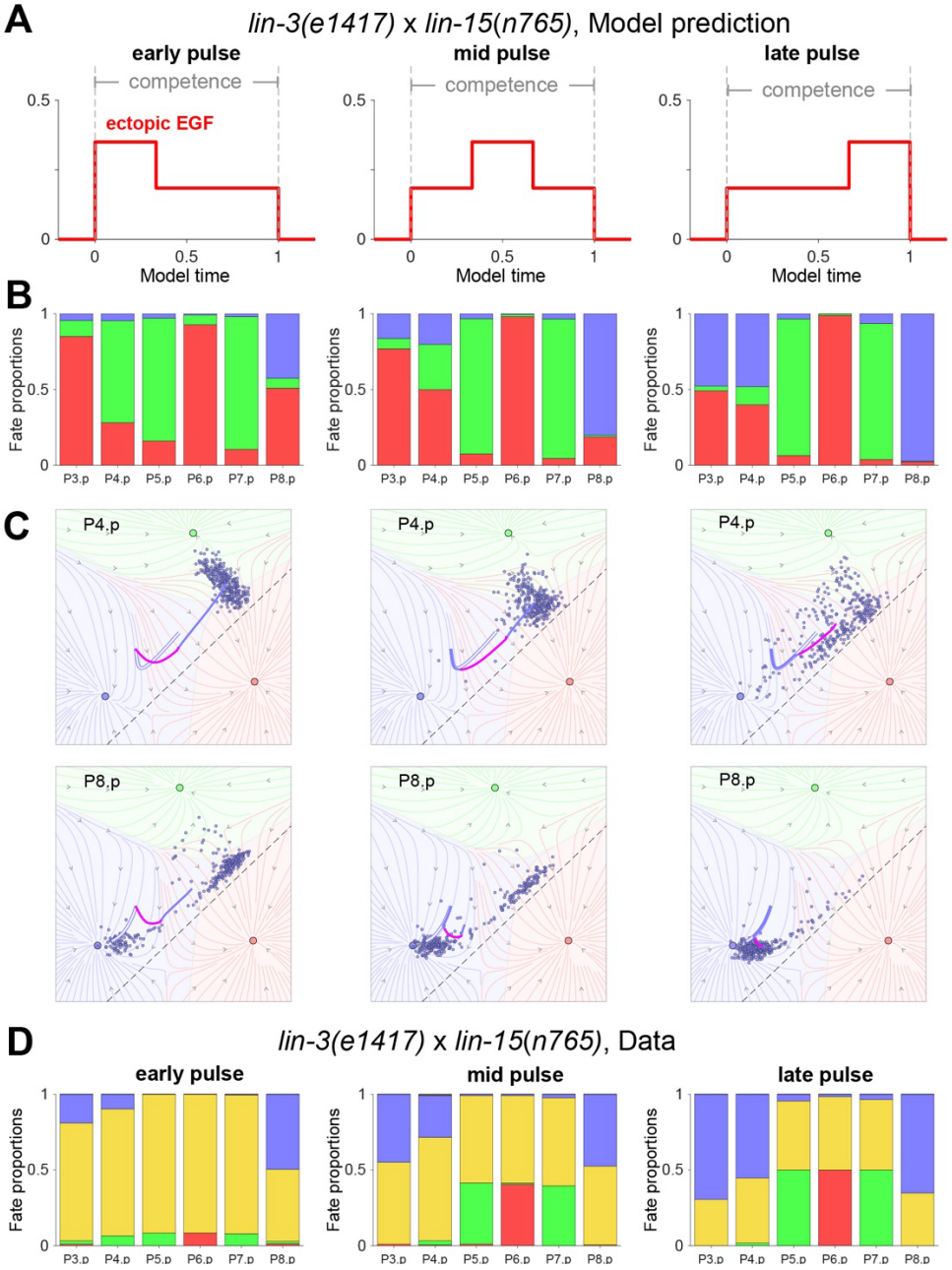


**Figure 5: Quantitative guiding of VPC fates with timed pulses of signaling activity in a background with reduced EGF from the AC.** (**A**) Temperature shifts at different times during competence in the *lin-3(e1417)* x *lin-15(n765)* double mutant are modeled as step-like increases and decreases in ectopic EGF, based on our fits for *lin-15(n765)* at 15ºC and 25ºC. (**B**-**C**) Predicted fate proportions (**B**) and fate trajectories of P4.p and P8.p (**C**). In (**C**), we depart from previous figures by overlaying the fate trajectories on a 'basal' flow field that includes the effect of the EGF signal received by each cell at 15º, i.e. $\vec{v}(\vec{r}, s_1\vec{m}_1)$ as per Eq. (1), with $s_1 = 0.2385$ for P4.p and $s_1 = 0.1585$ for P8.p, based on our fits for reduced EGF from the AC in *lin-3(e1417)* and ectopic EGF in *lin-15(n765)* at 15ºC. In each panel, the portion of the average trajectory corresponding to the pulse is highlighted in magenta, and the average trajectory in the absence of a pulse is shown as a white curve with a blue outline. This representation illustrates our interpretation of the outcomes based on the position of the cells at the end of the pulse and dynamics after the down-shift, e.g. an early pulse pushes (on average) P8.p to the separatrix (interface between blue trajectories ending in 3º and red trajectories ending in 1º) that exists at 15ºC, such that cells subsequently go to a mixture of 3º and 1º fates. (**D**) The corresponding experimental fate proportions show a stronger induction following early pulses, as predicted.

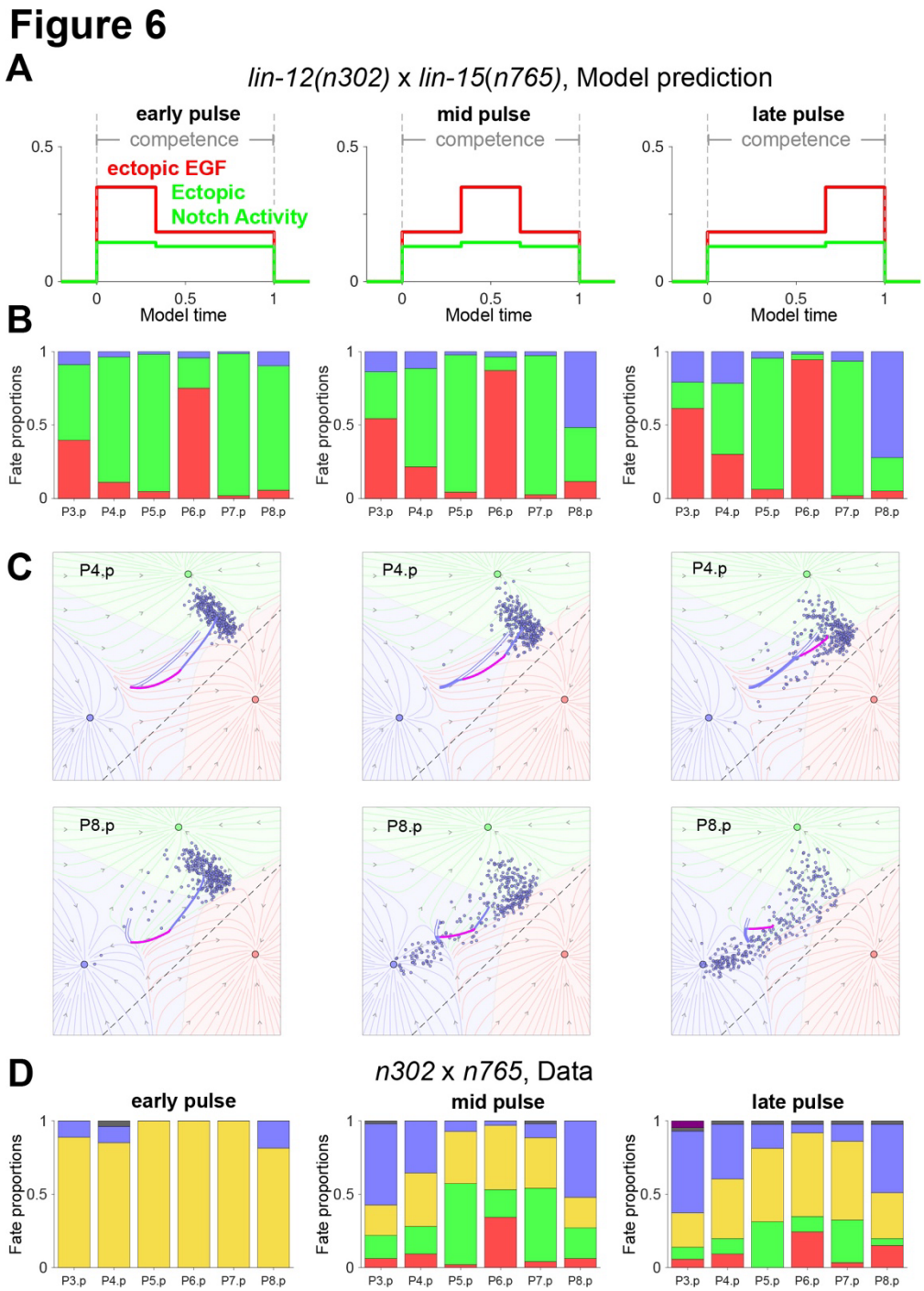


**Figure 6: Quantitative guiding of VPC fates with timed pulses of signaling activity in a background with ectopic Notch activity.** (**A**) Temperature shifts at different times during competence in the *lin-12(n302)* x *lin-15(n765)* double mutant are modeled as step-like increases and decreases in signaling activities, based on our fits for the two alleles at 15ºC and 25ºC. (**B**-**C**) Predicted fate proportions (**B**) and fate trajectories of P4.p and P8.p (**C**). Similar to Fig. 5, the fate trajectories in (**C**) are overlaid on a 'basal' flow field that includes the effect of the EGF signal and ectopic Notch signal received by each cell at 15º, i.e. $\vec{v}(\vec{r}, s_1\vec{m}_1 + s_2\vec{m}_2)$ as per Eq. (1), with $s_1 = 0.2328$ for P4.p and $s_1 = 0.1528$ for P8.p, and $s_2 = 0.13$ for both cells, based on our fits for residual EGF from the AC and constitutive Notch activity in *lin-12(n302)*, and ectopic EGF in *lin-15(n765)*, at 15ºC. (**D**) The corresponding experimental fate proportions show a stronger induction following early pulses, as predicted.

# Supplementary Figures

## Supplementary Figure 1

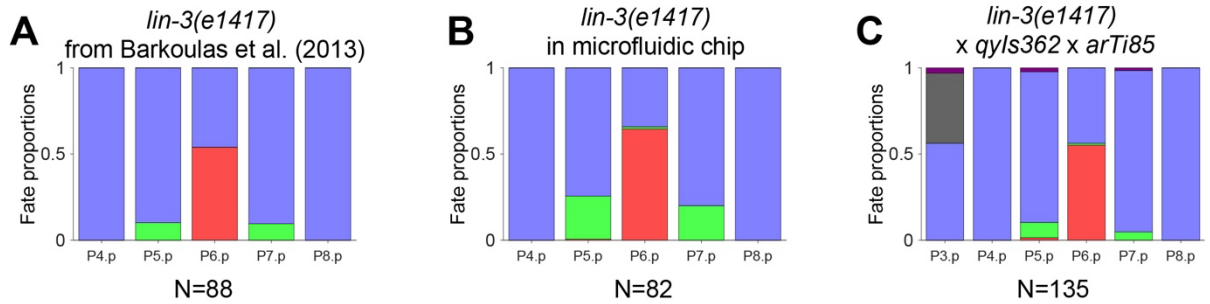


**Supplementary Figure 1: The AC marker *qyIs362* and the ERK biosensor *arTi85* do not influence VPCs fate decisions.** To assert whether AC marker *qyIs362* and ERK biosensor *arTi85* affect either EGF or Notch pathway activity in VPCs, we crossed these transgenes into the *lin-3*(*e1417*) sensitized background. The allele was previously fitted as $\lambda = 0.28$ (see Eq. (2)) based on data from [53] (**A**). We observed almost identical fate proportions for *e1417* when scored from animals developing in a previously published microfluidic device [45], showing that *e1417* is robust with respect to environmental conditions (see also [53,54]) (**B**). Any perturbation in the EGF or Notch signaling pathways are predicted to dramatically change the fate proportions as changes in $l_1$ or $l_2$ (representing EGF and Notch ligand levels) by only 0.05, for example, would lead to either 0% P6.p induction or double the induction levels of P5/7.p. However, when crossed into the two fluorescent reporters (**C**), parameter fits placed this strain within the confidence intervals of *e1417*. This is consistent with the hypothesis that EGF emission from the AC and MAPK & Notch pathway activities in VPCs are not affected by the *arTi85* and *qyIs362* transgenes.

## Supplementary Figure 2

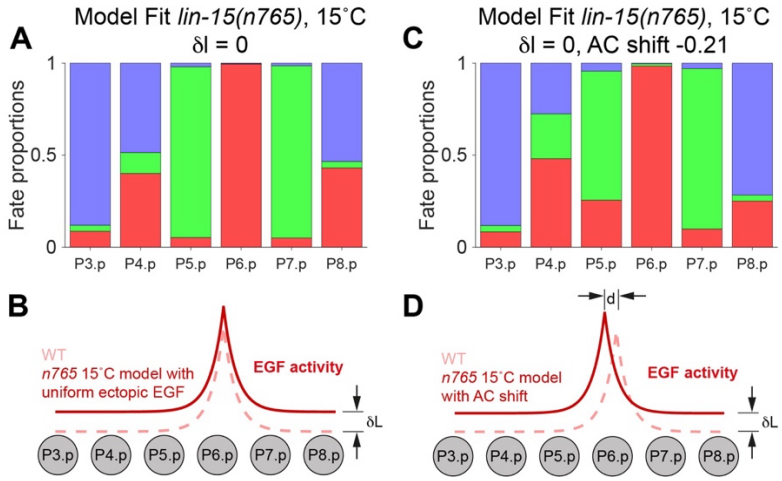


**Supplementary Figure 2: AC position shift cannot account for fate proportions in *lin-15(n765)*.** (**A, B**) Fate proportions in the model fit to *lin-15(n765)* at 15ºC with uniform ectopic EGF ($\delta l = 0$) and no AC shift (**B**), showing comparable induction levels for P4.p and P8.p (**A**). (**C**,**D**) With the AC shifted by 20% of the distance from P6.p to P5.p (**D**), the model can account for the asymmetric induction of P4.p and P8.p (**C**), but predicts only ~ 15% induction for P3.p. compared to > 50% in experiments (compare with main Fig. 2).

## Supplementary Figure 3

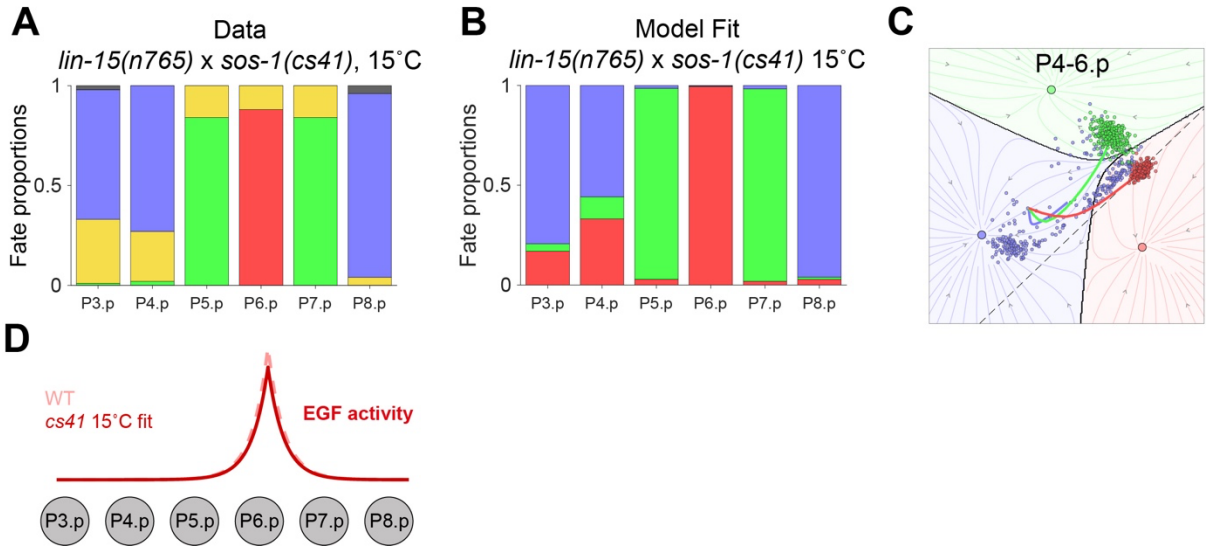


**Supplementary Figure 3: Using a cross to fit the *sos-1*(*cs41*) allele at the permissive temperature** (**A**-**B**) Experimentally observed fate proportions in the *lin-15*(*n765*) x *sos-1(cs41)* double mutant at 15ºC (N=50), and the corresponding fate proportions (**B**) and fate trajectories (**C**) in the model. Ectopic EGF levels in the model are taken from our fit to *lin-15(n765)* alone (see main Fig. 2), and the fold-change in EGF activity associated with *sos-1(cs4)* (**D**) is inferred from the phenotype of the cross in **A**.

## Supplementary Figure 4

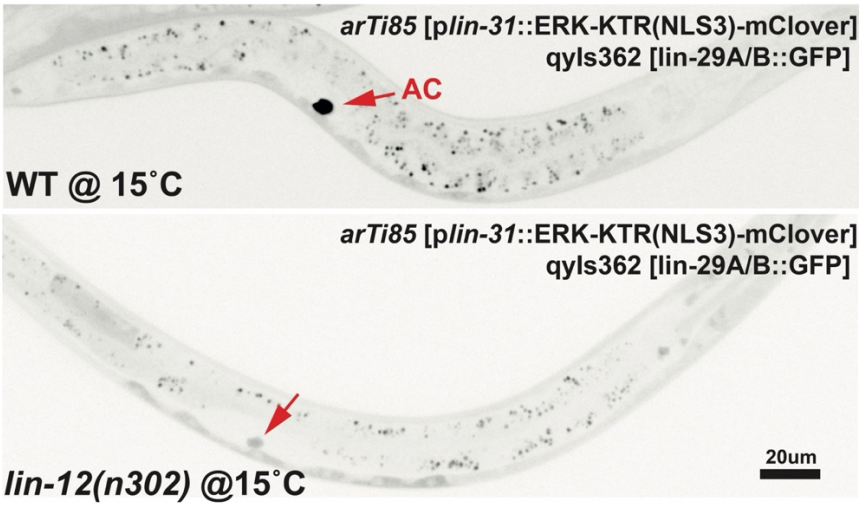


**Supplementary Figure 4: *lin-12(n302)* animals at 15˚C transiently express the AC marker *qyIs362* until the late L2 stage.** (Top) WT late L2 stage animal with bright expression of *qyIs362* (arrow). (Bottom) *lin-12(n302)* late L2 stage animal with faint but visible expression of *qyIs362*. Both images were taken at equal exposure time and laser power.

## Supplementary Figure 5

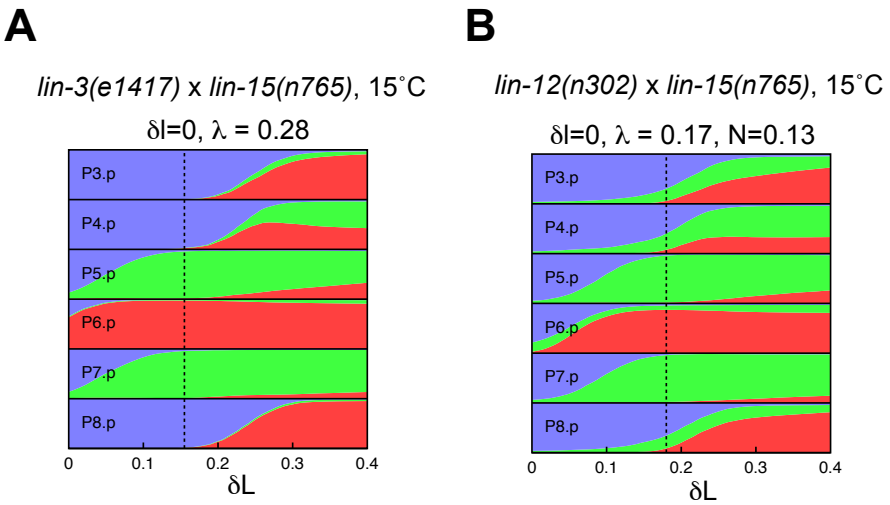


**Supplementary Figure 5:** (**A,B**) Fate proportions in the model as a function of ectopic EGF level $\delta L$ with uniform ectopic EGF ($\delta l = 0$), predicted for *lin-3(e1417)* x *lin-15(n765)* at 15˚C (**A**) and *lin-12(n302)* x *lin-15(n765)* at 15˚C. Dashed lines show our fits for the ectopic EGF level in *lin-15(n765)* at 15ºC.

## Supplementary Figure 6

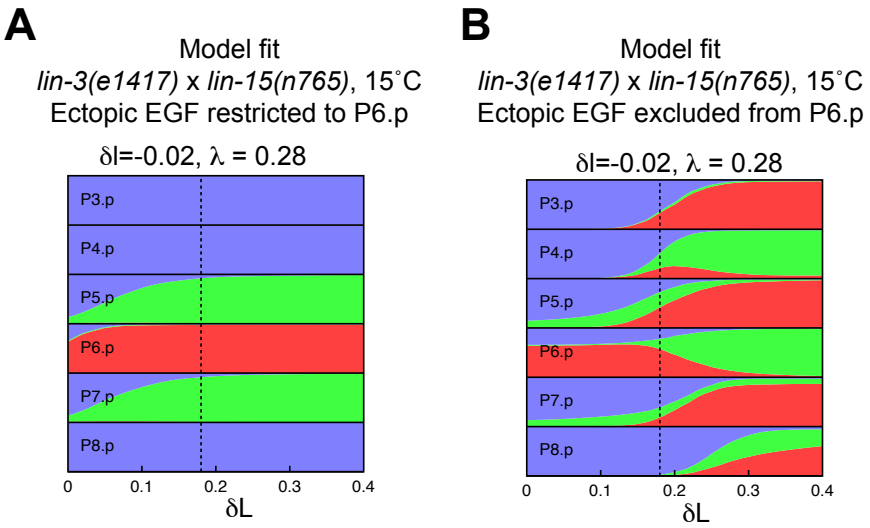


**Supplementary Figure 6: Contributions of direct vs. indirect signaling to rescue of *lin-3(e1417)* by ectopic EGF.** (**A**,**B**) Predicted fate proportions in the model as a function of ectopic EGF level in the *lin-3(e1417)* background, with ectopic EGF restricted to P6.p (**A**) or excluded from P6.p (**B**), to be compared with main Fig. 4A (ectopic EGF on all cells). Dashed lines show our fit for the ectopic EGF level in the *lin-15(n765)* mutant at 15ºC. In the absence of ectopic EGF signaling in P5,7.p (**A**), the stronger Notch signal received from P6.p (which itself receives a higher EGF signal) is sufficient to account for the near-complete rescue of P5-7.p to their WT fates, as seen in simulations with unrestricted ectopic EGF (main Fig. 4A-C) and in experiments (main Fig. 4D). By contrast, in the absence of additional Notch signaling from P6.p (**B**), the ectopic EGF received directly by P5,7.p themselves only partially rescues induction of P5,7.p (**B**), and results in the induction of 1º as well as 2º fates.

# Supplementary Figure 7

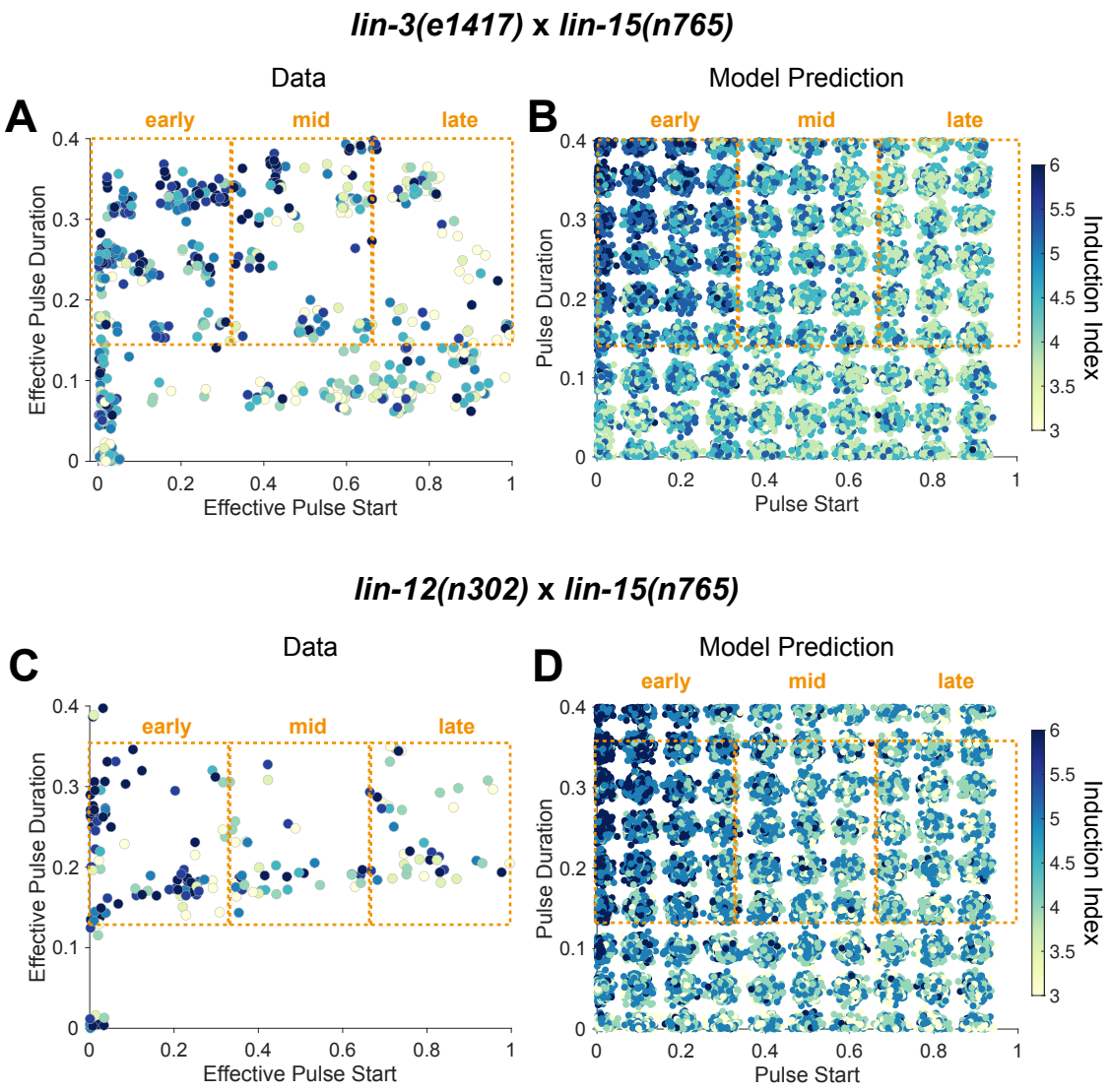


**Supplementary Figure 7:** (**A**,**B**) Experimentally observed vulval induction levels (**A**; N=610) and model predictions (**B**) as a function of pulse start time and duration in the *lin-3*(*e1417)* x *lin-15*(*n765)* double mutant. Notice that induction levels decrease on average for pulses occurring later in the competence period. (**C**,**D**). Same as (**A**,**B**) for the *lin-12(n302)* x *lin-15(n765)* double mutant (N=309). Effective start times and durations in (**A**,**C**) are normalized to the duration of the competence period (see Materials & Methods). Dashed orange rectangles indicate which animals were included in the early-, mid-, and late-pulsed populations in main Figs. 5 and 6.